International Journal of Lightweight Materials and Manufacture 7 (2024) 914–924

Contents lists available at ScienceDirect

International Journal of Lightweight Materials and Manufacture

journal homepage: www.keaipublishing.com/ijlmm

Original Article

Integrated Taguchi-PCA-GRA based multi objective optimization of tube projection and radial clearance for friction stir welded heat exchanger tube-to-tube sheet joints

Dinu Thomas Thekkuden [a], Muhammad M. Sherif [b], Mohammad Alkhedher [a], Syed Haris Iftikhar [c], Abdel-Hamid Ismail Mourad [c, d, e, *]

[a] Mechanical and Industrial Engineering Department, Abu Dhabi University, 59911, Abu Dhabi, United Arab Emirates
[b] Civil, Construction and Environmental Engineering Department, School of Engineering, University of Alabama at Birmingham, Birmingham, USA
[c] Mechanical and Aerospace Engineering Department, College of Engineering, United Arab Emirates University, Al-Ain, P.O. Box. 15551, United Arab Emirates
[d] National Water and Energy Center, United Arab Emirates University, Al Ain 15551, United Arab Emirates
[e] On Leave from Mechanical Design Department, Faculty of Engineering, El Mataria, Helwan University, Cairo, Egypt

ARTICLE INFO

Article history:
Received 24 January 2024
Received in revised form
25 May 2024
Accepted 29 May 2024
Available online 4 June 2024

Keywords:
Heat exchanger
Leak path
Pull-out strength
Friction stir welding
Tungsten inert gas welding

ABSTRACT

Leak proof tube-to-tube sheet joints are mandatory for the optimal operation and longevity of the shell and tube heat exchanger. Tube-to-tube sheet joints play a crucial role as fluid barriers, ensuring effective separation between the tube and shell side fluids within shell and tube heat exchangers. Non-conventional friction stir welding, known for imparting less residual stresses, is not commercially used for the fabrication of tube-to-tube sheet joints due to complex joint configuration and geometrical limitations. An extensive study on friction stir welding considering the geometrical parameters of tube-to-tube sheet arrangement is highly demanded. This research examined the mutual influence of radial clearance ranging from 0 mm to 0.5 mm and tube projection lying from 1 mm to 2 mm in friction stir welding of tube to tube sheet configuration on the pull-out strength, extension and, hardness at the stirring and fusion zones. Optimum radial clearance and tube projection for achieving high mechanical weld properties was estimated using multi-objective integrated Taguchi-PCA-GRA optimization. The result proves that the friction stir welded joint is capable of achieving joint strength close to the tungsten inert gas welded joint. The optimum parameters are 2 mm for tube projection and 0 mm for radial clearance to achieve maximum strength and weld penetration, while minimizing hardness at both stir zone and fusion zone. The findings of this research proved the adaptability of friction stir welding for the fabrication of tube-to-tube sheet joints with the right choice of tube projection and radial clearance.

1. Introduction

The shell and tube heat exchanger (STHE) market size is anticipated to expand at a 7.5% compound annual growth rate (CAGR) from 2022 to 2029, rising from USD 16.64 billion to USD 27.55 billion. In comparison to various types of heat exchangers such as plate-fin heat exchanger, air coolers, cooling towers and others, the STHEs are dominated with 33% of reliability and use. Industries dealing with chemicals, petrochemicals, food and beverages, HVAC and refrigeration, pulp and paper, power generation heavily use the STHEs. Due to the high market demand and wide-scale applicability of STHEs, manufacturers and researchers have gained interest to understand and optimize their manufacturing processes, maintenance and operation conditions.

Aluminum alloys are preferred for heat exchangers that are exposed to acidic environments due to their inherent corrosion resistance. Aluminum heat exchangers are used for automotive, marine, chemical processing and food processing applications. The benefits of aluminum STHEs are due to their light weight, flexibility, high thermal efficiency and cost-effectiveness. Moreover, aluminum, is the third highest thermal conductive material, with

* Corresponding author. Mechanical and Aerospace Engineering Department, College of Engineering, United Arab Emirates University, Al-Ain, P.O. Box. 15551, United Arab Emirates.

E-mail address: ahmourad@uaeu.ac.ae (A.-H.I. Mourad).

Peer review under the responsibility of Editorial Board of International Journal of Lightweight Materials and Manufacture.

https://doi.org/10.1016/j.ijlmm.2024.05.010

Fig. 1. Word cloud generated from Scopus database using articles dealing with **TTSJs**.

approximately 237 W/(m.K). Also, aluminum alloys exhibit high strength with a slight reduction in thermal conductivity 160 W/(m.K).

Recent research of tube-to-tube sheet joints (TTSJs) were case studies of defected heat exchanger that developed analytical and numerical methodologies for estimating the contact pressure and residual stresses. Fig. 1 illustrates the generated word cloud based on the data extracted from Scopus database considering the published articles related to TTSJs. The larger the size of the text in the word cloud indicates the maximum occurrences of keywords in the articles. Tubes, expansion process, corrosion phenomenon, welding, pressure, and residual stress are major points of research interest. As such, manufacturing processes mainly welding and tube expansion proved the demand for investigating the manufacturing processes.

The manufacturing of TTSJs in STHE is highly critical. The commercialized conventional manufacturing methods to produce the tube-to-tube sheet joints are tube expansion process and welding. Tube expansion process comprises of roller expansion process, hydraulic expansion process and explosion expansion process. In the case of welding, tungsten inert gas welding is a widely chosen process. It is also common to use both welding and expansion either welding followed by expansion or expansion followed by welding for producing TTSJs. Based on these processes, the TTSJ is classified into expanded, seal welded and strength welded joints configuration [1]. Any defective joint developed at the manufacturing stage or operation stage will lead to a malfunction in the heat exchanger. The traditional welding approach for producing TTSJs is tungsten inert gas (TIG) welding process and the schematic description is provided in Fig. 2. The leakage between the tube and tube sheet is one of the reasons for the sudden ceasing of the STHEs [2]. The failure analysis of STHE exposed to H_2S environment indicated that the vibration, using of seal welding, tube expansion before welding and poor weld quality were the potential reasons for the leakage at the TTSJ [3]. Lack of weld penetration in tube-to-tube sheet welds by tungsten inert gas welding process is another major reason for leakage at the TTSJ [4]. Welding trials for setting up optimized welding parameters and welding procedure specification are mandatory before implementing the parameters for joining the final components [5,6]. In addition to lack of weld penetration by the TIG process, poor weld workmanship also results in poor quality TTSJs [7]. High residual stress at the weld toe of gas tungsten inert gas welded TTSJs favors crack initiation [8]. In another case, stress corrosion cracking due to high residual stress and flawed welds were the reasons for the failure of waste heat boiler [9]. For many decades until present, the tube-to-tube sheet welds were manufactured by only tungsten inert gas welding process. TIG welding followed by tube expansion process using either of roller expansion or hydraulic expansion equipment are also traditionally practiced for fabricating strengthened joints [10]. However, there are no alternative welding techniques currently being commercialized and used for fabricating TTSJs. For these reasons, a green manufacturing technique with leak proof seal that imparts minimized heat input and residual stress for TTSJ application has the potential to revolutionize the heat exchanger industry. Friction stir welding (FSW) has been proven for joining similar shaped components such as plate-to-plate [11–16], pipe-to-pipe [17–23] and T joints [24,25]. Therefore, the capability of friction stir welding-based manufacturing process for TTSJs (complex or dissimilar shaped geometry) in STHE is evaluated in this research.

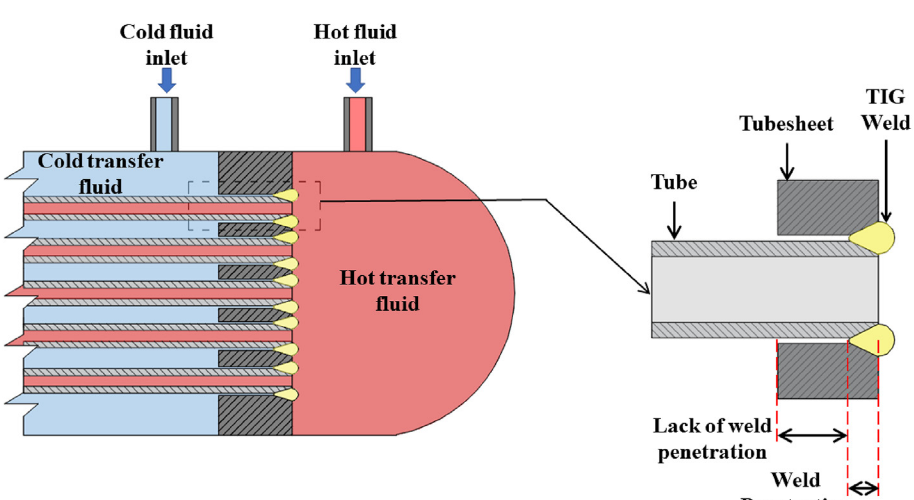

Fig. 2. Tungsten inert gas welded TTSJs in STHE.

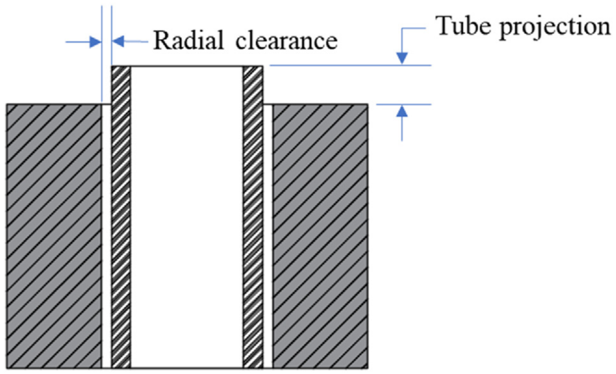

Fig. 3. Schematic diagram showing radial clearance and tube projection.

Tube and plate, being two different complex geometry, are joined together by softening the adjoining region coming in contact with the rotating and plunging tool. The joint strength is one of the main quality measures for qualifying the welded joints especially in the heat exchangers that are exposed to high operating pressures. The joints need to withstand the operating pressure, otherwise the leakage initiates at the TTSJs. Therefore, the main criteria of the quality friction stir welded tube to tube sheet joints are the joint strength [26]. However, the FSW of tube to plate was found not viable for tubes with inner diameter less than 7.5 mm due to evolvement of joint cracks that caused significant depreciation in the strength of the joints [27]. Friction-stir welds with tube projected out from the plate surface by 0 mm, 3 mm and 4 mm were found inappropriate due to the presence of continuous cracks along the weld interface. However, the optimal condition of tube projection was 1 mm and 2 mm for defect-free joints [28]. The tube projection is the projected tube from the tube sheet surface whereas the radial clearance is the clearance gap between the tube and tube sheet as illustrated in Fig. 3. The authors have proved that a minimum of 1 mm tube projection is necessary for filling the radial clearances of 0.5 mm with a weld penetration of 4.6 mm [29]. Furthermore, the optimal process parameters for friction stir welding of tube-to-plate are 1500 rpm rotational speed, 2 mm tube projection and 1.5 mm penetration depth [28]. In the friction stir welding of dissimilar admiralty brass C44300 to AA7075-T651 aluminum plate, the thread on the outer tube surface in contact with the plate had an optimum pitch be 1.5 mm over the range of 0.5 mm−1.5 mm [30]. A constant clearance fit of 0.1 mm was used between copper tube and AA 2025 plate for the friction stir welding of tube to plates [31]. Until present, the investigated factors were tube projection, thread on the tube, holes on the tube, inner tube diameter, rotational speed of the tool, plunging depth and clearance.

In reality, the clearance between the tube and tube sheet ought to increase by more than 0.1 mm. The tubes are needed in STHEs to insert through two tube sheets placed at the two ends and many baffles between the tube sheets depending on the length of heat exchanger. For the easy insertion of the tube through baffles and tube sheets, the radial clearance between the tube and tube sheet holes should be greater than 0.1 mm. The determination of radial clearances is considered an important criterion in the designing stage of STHEs. The uneven outer tube diameter and tolerances during tube production also cater the need for considering the radial clearances between the tube and tube sheet hole.

Literatures describing the investigation of two key parameters such as tube projection and radial clearance on the joint characteristics of tube to plate joints are considerably less reported. Radial clearance, being an important factor in STHEs, needs a systematic evaluation for finding the optimum condition and feasible range for the FSW process. Therefore, the main objectives of this research are to investigate the mechanical characteristics of friction stir welded TTSJs, optimization using integrated Taguchi-PCA-GRA and metallurgical observation of the optimum selection of tube projection and radial clearance.

2. Materials and methodology

TTSJs made of AA 6061-T6 tube and AA 6063-T6 tube sheet are manufactured using friction stir welding and tungsten inert gas welding processes. Table 1 and Table 2 provide the chemical composition of AA 6061-T6 and AA 6063-T6 materials estimated using optical emission spectroscopy. The average tensile strength of AA 6061-T6 tube and AA 6063-T6 tube sheet after performing tensile test with two replications of the samples are 266.63 MPa and 237.29 MPa respectively whereas the yield strength of AA 6061-T6 tube and AA 6063-T6 tube sheet are 249.58 MPa and 213.22 MPa respectively. Table 3 shows the chemical composition for the FSW tool made of H13 tool steel that is used for generating heat due to friction at the tool shoulder to specimen interface. The H13 tool steel was chosen based on the applicability of the material for friction stir welding process [32,33]. Fig. 4a presents the tool used for the friction stir welding process. Unlike the conventional FSW tool, the tool is designed to have a tool guide and shoulder. The purpose of the tool guide is to align the tool axis to the axis of the

Table 1
Chemical composition of AA 6061 pipe using optical emission spectroscopy (%).

Si	Fe	Cu	Mn	Mg	Cr	Ni	Zn
0.413	0.13	0.0015	0.0292	0.487	0.0075	0.0035	0.0026
Ti	**B**	**Ba**	**Be**	**Ca**	**Cd**	**Ga**	**Hg**
0.0101	0.00053	0.00042	0.00023	0.0081	0.00063	0.008	<0.00089
Li	**Na**	**P**	**Pb**	**Sn**	**V**	**Zr**	**Al**
<0.00003	0.0122	<0.00009	0.001	0.00096	0.0109	0.00043	98.9

Table 2
Chemical composition of AA 6063 plate using optical emission spectroscopy (%).

Si	Fe	Cu	Mn	Mg	Cr	Ni	Zn
0.404	0.177	0.0021	0.0338	0.481	0.0033	0.0035	0.0074
Ti	**B**	**Ba**	**Be**	**Ca**	**Cd**	**Ga**	**Hg**
0.0081	0.00018	0.00044	0.00032	0.008	0.00051	0.0108	<0.00078
Li	**Na**	**P**	**Pb**	**Sn**	**V**	**Zr**	**Al**
<0.00008	0.0063	<0.00005	0.0022	0.00076	0.0117	0.0006	98.9

Table 3
Chemical composition of H13 tool steel using optical emission spectroscopy (%).

C	Si	Mn	P	S	Cr	Mo	Ni
0.395	0.927	0.357	0.0088	0.0081	5.33	1.26	0.0913
Al	**Co**	**Cu**	**Nb**	**Ti**	**V**	**W**	**Pb**
0.06	0.0252	0.078	0.0146	0.0154	0.927	0.0119	0.0175
Sn	**As**	**Zr**	**Bi**	**Ca**	**Ce**	**Sb**	**Se**
0.0042	<0.008	0.0023	0.0162	0.00094	0.0077	0.007	<0.0011
Te	**Ta**	**B**	**Zn**	**La**	**N**	**Fe**	**CEV**
>0.0457	0.0204	0.0027	0.004	0.00065	>0.0306	90.3	1.97

tube, henceforth, the tool guide is cylindrical, and the surface of the tool guide is smooth. Friction stir welding is performed using a vertical milling machine at a constant 1600 rpm and 0.4 mm plunge depth, as illustrated in Fig. 4b. Tungsten inert gas welding was performed using ER5356 filler and Kemppi power source with 53 A and 10.3 V. The TIG welded samples are shown in Fig. 5. The chemical composition and mechanical properties of ER 5356 is shown in Table 4.

The dimensions of tube were outer diameter of 18 mm, inner diameter of 13 mm and tube wall thickness of 2.5 mm. The tubes were cut with a length of 51 mm, 51.5 mm and 52 mm. The tube sheet was 50 × 50 × 5 mm plate with a drilled hole at the center. Specimens with hole diameter of 18 mm, 18.5 mm and 19 mm were fabricated for radial clearances of 0 mm, 0.25 mm and 0.5 mm between the tube and tube sheet. A 50 × 50 × 45 mm fixture with 18 mm drilled hole was used to place the tube and tube sheet firmly. The total height of the fixture with tube sheet is 50 mm. The tube lengths of 51 mm, 51.5 mm and 52 mm left the protruded tube from the tube sheet surface with a length of 1 mm, 1.5 mm and 2 mm, respectively. Taguchi-based L9 orthogonal array experimental design using 2 factors and 3 levels was generated in Minitab as described in Table 5. Fig. 6 displays samples of the friction stir welded coupons. Table 6 describes the response of the friction-stir welded coupons in-terms of tube pull-out load, maximum extension, hardness at stirring and fusion zone.

A fixture was designed to hold the tube-to-tube sheet coupon as the grip spacing in universal testing machine for tube pull-out testing was limited to 15 mm as illustrated in Fig. 7a. The 18 mm outer tube diameter and 50 mm tube sheet plate thickness clearly exceeded the maximum grip width of 15 mm. The peak load and maximum extension were collected from the load-displacement curve. For microstructural analysis, the sectioned friction stir welded surface has been ground using SiC papers (P120 to P1200) and polished with 9 μm alumina-water solution. Polished samples are etched using Keller's reagent for 30 s. The microstructure of friction-stir welded joints is evaluated using Panthera TEC MAT

Table 4
Chemical composition of ER5356 TIG electrode [34].

Mn	Si	Cr	Al	Cu	Zn	Fe	Mg
0.13	0.05	0.12	94.56	0.01	0.01	0.13	4.9
Tensile Strength: 265 MPa			Yield strength: 120 MPa			Elongation: 26%	

microscope. The Vickers hardness at the stirring zone (SZ) and fusion zone (FZ) are illustrated in Fig. 7b and c, respectively, and were measured using a Wilson UH250 Universal Hardness Tester at a test load of 10 kgf.

3. Multi-objective optimization: Taguchi-PCA-GRA

Step 1: Determining the SN ratio using Taguchi analysis.

Step 2: The SN ratios of responses are normalized to represent values between 0 and 1. Eq. (1) is used for larger the better (objective is maximizing the response) and Eq. (2) is used for smaller the better (objective is minimizing the response).

$$x_i(k) = \frac{y_i(k) - \min y_i(k)}{\max y_i(k) - \min y_i(k)} \quad (1)$$

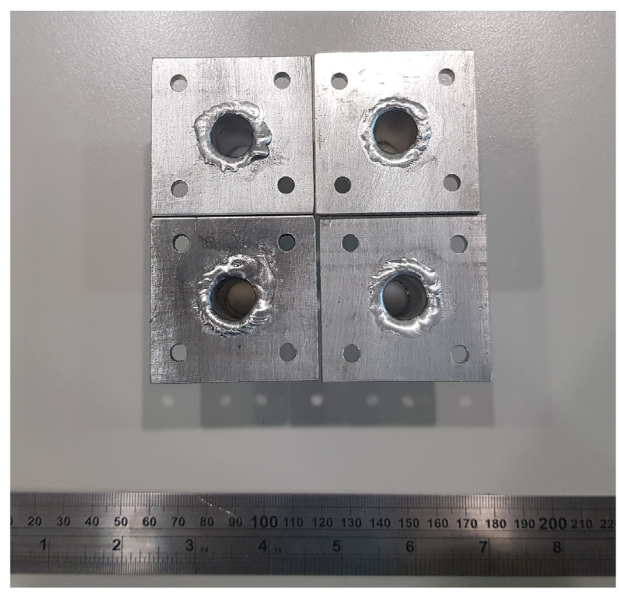

Fig. 5. Tungsten inert gas welded tube to tube sheets.

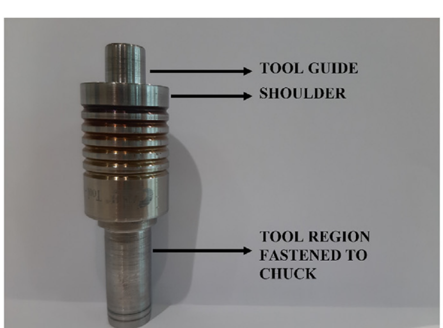

(a)

(b)

Fig. 4. (a) Friction-stir welding tool designed for joining tube-to-tube sheet using tool shoulder, and (b) Friction-stir welding using vertical milling machine and friction stir welding tool.

Table 5
Factors and levels of projection length and radial clearance.

Parameters	Symbol	Units	Level 1	Level 2	Level 3
Projection	PL	mm	1	1.50	2.00
Radial Clearance	RC	mm	0	0.25	0.50

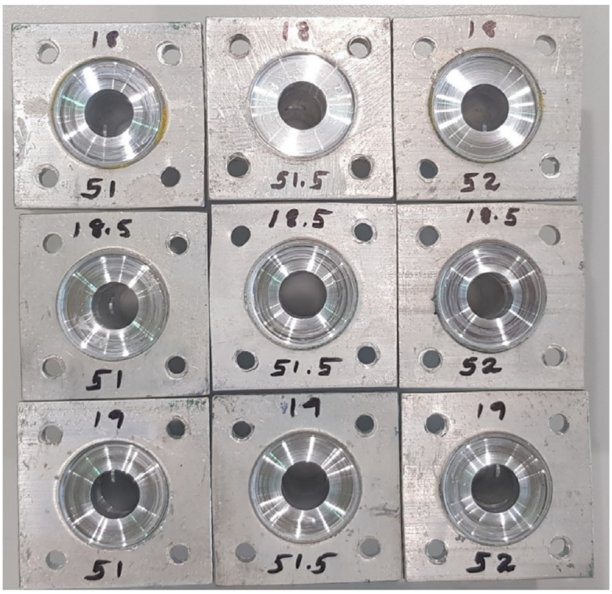

Fig. 6. Friction-stir welded coupons.

$$x_i(k) = \frac{\max y_i(k) - y_i(k)}{\max y_i(k) - \min y_i(k)} \quad (2)$$

Where, x$_i$)k(is the normalized value of response, least value of y$_i$)k(is min y$_i$)k(and highest value of y$_i$)k(is max y$_i$)k(for kth response.

Step 3: Calculate the grey relational coefficient using Eq. (3).

$$\zeta_i(k) = \frac{\Delta_{min} + \psi\, \Delta_{max}}{\Delta_{oi}(k) + \psi\, \Delta_{max}} \quad (3)$$

Where, $\Delta_{oi}(k) = |x_0(k) - x_i(k)|$, chosen Ψ, distinctive coefficient is 0.5.

Step 4: The grey relational coefficients are arranged in a linear combination array forming a matrix (Eq. (4)).

$$y = \begin{bmatrix} y_1(1) & y_2(2) & \cdots & y_1(k) \\ y_2(1) & y_2(2) & \cdots & y_2(k) \\ \cdots & \cdots & \cdots & \cdots \\ y_j(1) & y_j(2) & \cdots & y_j(k) \end{bmatrix} \quad (4)$$

where $y_p(q)$ is the grey relational coefficients of each quality responses, $p = 1, 2, \ldots j$, experiments, and $q = 1,2, \ldots k$, quality responses. In this study, experiment runs, j = 9 and number of responses, k = 4.

Step 5: Generate correlation matrix using Eq. (5).

$$R_{jl} = \left(\frac{Cov\left(y_p(q), y_p(l)\right)}{\sigma_{yp}(q) * \sigma_{yp}(l)}\right) q = 1, 2, \ldots, k;\; l = 1, 2, \ldots, k \quad (5)$$

where the covariance of the sequences $y_p(q)$ and $y_p(l)$ is denoted by Cov($y_p(q)$, $y_p(l)$). The standard deviation of sequence $y_p(q)$ is $\sigma_{yp}(q)$ and the standard deviation of sequence $y_p(l)$ is $\sigma_{yp}(l)$.

Step 6: The eigenvalues and eigenvectors are evaluated using R_{jl} array as shown in Eq. (6).

$$(R - \lambda_k I_j)\, V_{pk} = 0 \quad (6)$$

Step 7: Eigenvalues (λ_k) and eigenvectors (V_{pk}) of square matrix R are used to determine the uncorrelated principal components (PC's) by using Eq. (7).

$$Z_{jk} = \sum_{i=1}^{n} \gamma_j(p)\; x\; V_{pk} \quad (7)$$

where the kth principal component is represented by Z_{jk}.

Step 8: The weights for each of the responses are calculated by squaring the eigenvectors of the first principal component.

Step 9: The grey relational grade is computed using Eq. (8).

$$\gamma_j\left(y_0^*, y_j^*\right) = \frac{1}{n} \sum_{q=1}^{n} w_q \xi\left(y_j^*(q), y_0^*(q)\right) \quad (8)$$

where the grey relational grade for jth experimental run is represented by $\gamma_j(y_0^*, y_j^*)$, number of quality response by n, weight of qth quality response by w_q and $\sum_{q=1}^{n} w_q = 1$.

4. Results and discussions

4.1. Tube pull-out strength

Tube pull-out test reveals the maximum load bearing capacity of the welded joint. Fig. 8 illustrates the maximum tube pull-out load (i.e., load bearing capacity) of the friction stir welded joints. The peak tube pull-out load of tungsten inert gas welded TTSJs were 7964.4 N, 10,081.84 N and 8403.86 N. The tube pull-out loads of tungsten inert gas welded joints were within the range of 7964.4 N and 10,081.84 N. A maximum tube pull-out force of 10,073.37 N was achieved for specimen with 2 mm tube projection and a 0 mm radial clearance using friction stir welding process. The difference of the maximum load bearing capacity between the FSWed and TIG welded joints was only 8.47 N. This proved that the

Table 6
Factors and levels of projection length and radial clearance.

Runs	Radial Clearance	Projection (mm)	Load (N)	Extension (mm)	Hardness Stirring Zone (HV)	Hardness Fusion Zone (HV)
1	0	1	8202.87	10.018	51.53	57.15
2	0	1.5	5176.91	4.448	54.32	53.69
3	0	2	10,073.37	13.890	50.26	52.87
4	0.25	1	6046.90	6.314	54.75	54.01
5	0.25	1.5	9648.47	11.051	56.43	54.615
6	0.25	2	6180.90	5.787	47.21	54.78
7	0.5	1	6603.89	5.127	50.07	51.48
8	0.5	1.5	7809.67	7.377	54.75	53.91

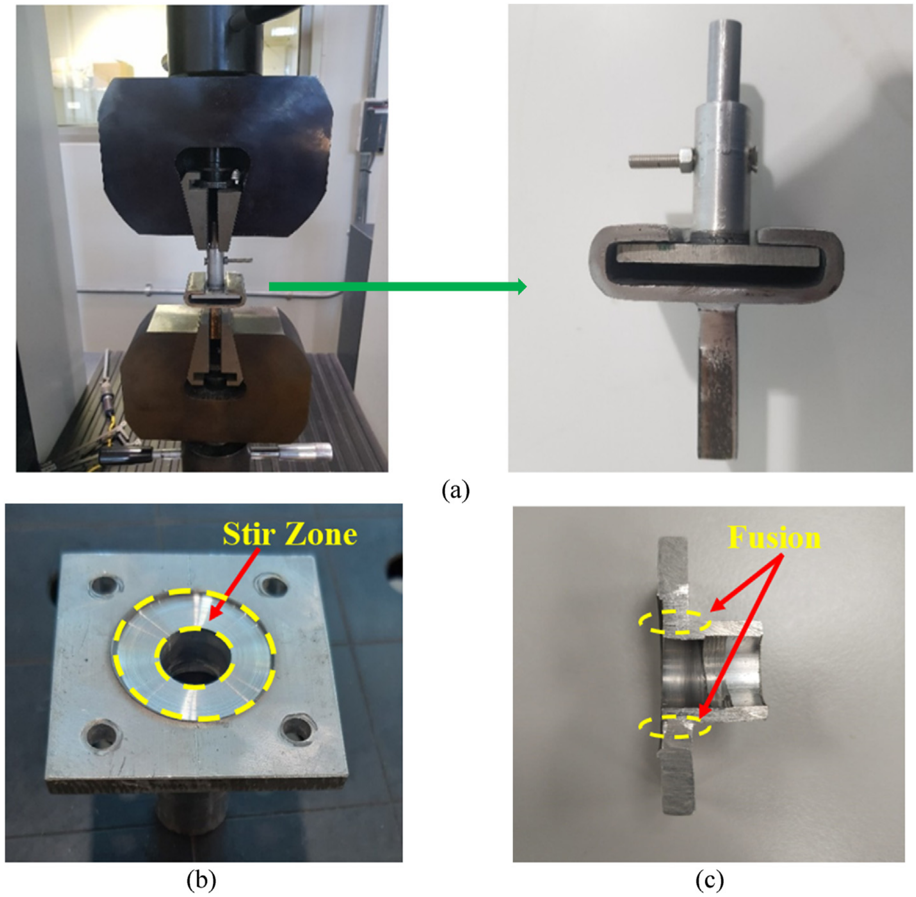

Fig. 7. (a) Developed fixture for performing tube pull-out test, zones at TTSJ (b) stir zone, and (c) fusion zone.

friction-stir welding process was successful in achieving maximum load bearing capacity that is similar to tungsten inert gas welding process. It was discovered that specimen with 1.5 mm tube projection and 0.25 mm radial clearance (9648.47 N), and specimen with 1 mm tube projection and 0 mm radial clearance (8202.87 N) were within the strength range of TIG-welded joints. Henceforth, friction stir welding technique was proved to produce strengthened joints using wise selection of tube projection and radial clearances.

Fig. 9 illustrates the main effect mean plot of tube projection and radial clearance on the pull-out load. The pull-out load increased sharply from 6951 N to 7545 N with an increase in the tube projection from 1 mm to 1.5 mm tube projection. However, further increase in the tube projection to 2 mm, slightly reduced the tube pull-out load to 7471 N. The marginal difference of tube pull-out load for tube projection between 1.5 mm and 2 mm is only 74 N. A protruded tube length greater than or equal to 1.5 mm is concluded as ideal for achieving maximum strength. In the case of radial clearances, there is an abrupt reduction of tube pull-out load when the radial clearance was increased from 0 mm to 0.5 mm. The maximum average pull-out load at 0 mm radial clearance was 7818 N. The tube pull-out load reduced to 7292 N for specimen with 0.25 mm radial clearance and further reduced to 6857 N for specimen with 0.5 mm radial clearance. It was found that the absence of radial clearance and tube projection of at least 1.5 mm resulted in the maximum tube pull out strength.

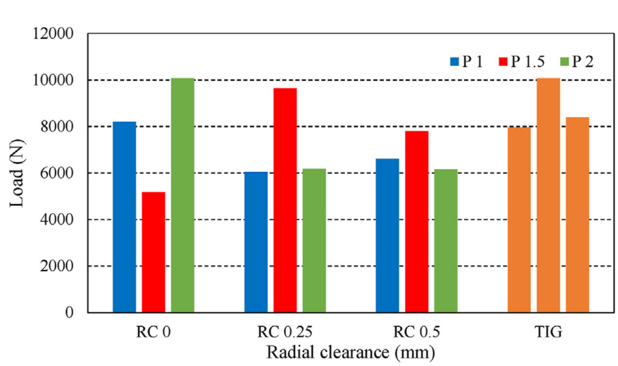

Fig. 8. Pull-out loads of FSW welded and TIG welded **TTSJs**.

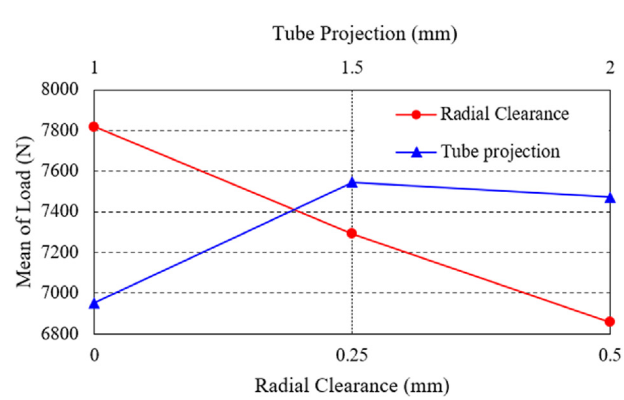

Fig. 9. Main effect plot of tube pull-out load.

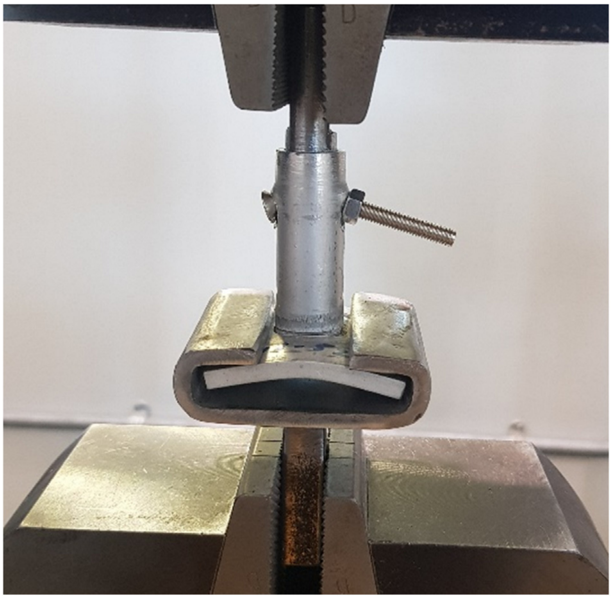

Fig. 10. Bending of the tube sheet under the action of pull-out load.

The bending of the tube sheet as illustrated in Fig. 10 indicate the capability of friction-stir welded joints to carry the tensile load. As a result, the maximum extension in the load versus displacement graph is considered as an indication of the ductile nature of the weld joint as shown in Fig. 11. The maximum load and extension increase the area under the load-displacement curve and represents the work done or the energy transferred. A weldment with higher extension is preferred for joints exposed to high pressure. The main effect plots of extension in Fig. 12 indicate that the linear declination from 9.45 mm at 0 mm radial clearance to 6.192 mm at 0.5 mm radial clearance. On the other side, the extension increased linearly from 7.15 mm to 8.58 mm when the tube projection was increased from 1 mm to 2 mm, respectively.

4.2. Hardness

The stirring zone was developed on the tube sheet by the interaction of rotating tool shoulder on the upper tube sheet and tube surfaces. The main effect plot for the stirring zone hardness is illustrated in Fig. 13. The mean hardness at the stirring zone for 1 mm tube projection was 52.12 HV. The hardness increased to 55.17 HV for 1.5 mm tube projection and reduced to exhibit the least hardness of 49.00 HV for 2 mm tube projection. It is noted that the mean hardness at the stirring zone was nearly constant averaging 52 ± 1 HV at each radial clearance for various tube projections. A sudden drop in the hardness at 2 mm tube projection is due to the softening of the material. This was caused by effective stirring on tube and tube sheet for prolonged time. The tool shoulder was continuously in contact with the tube until the tube softened up to 2 mm before in contact with the tube sheet. The tube was subjected to thermo-mechanical interaction for softening of the protruded tube. The hardness at the stirring zone decreases with the increased softening behavior. However, the mean hardness at 1.5 mm tube projections was found to be the highest when compared to 0 mm and 2 mm tube projections.

The main effect plot of hardness at the fusion zone, formed at the gap between the tube and tube sheet is shown in Fig. 14. The

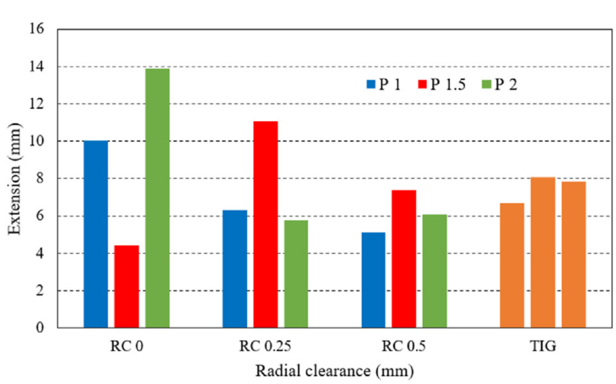

Fig. 11. Maximum extension during tube pull-out test.

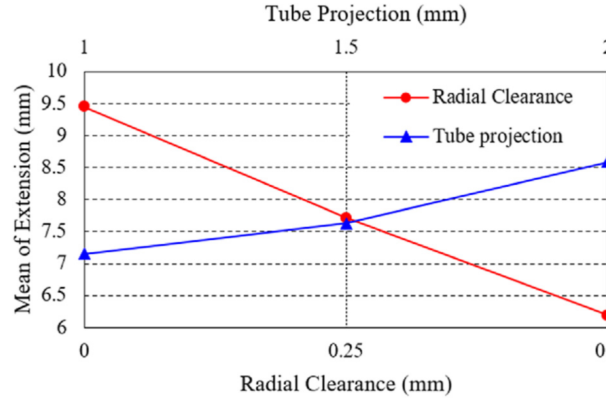

Fig. 12. Main effect plot of extension.

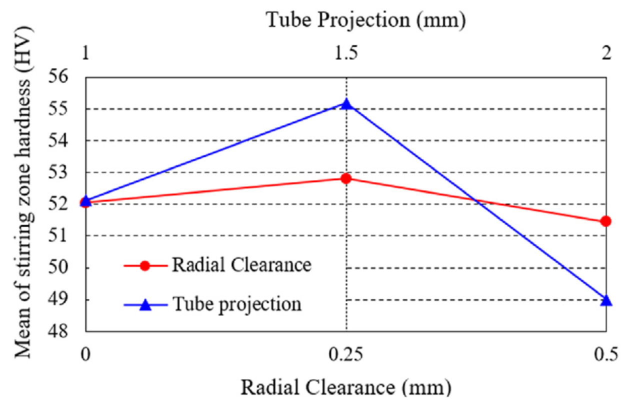

Fig. 13. Main effect plot of hardness at stirring zone.

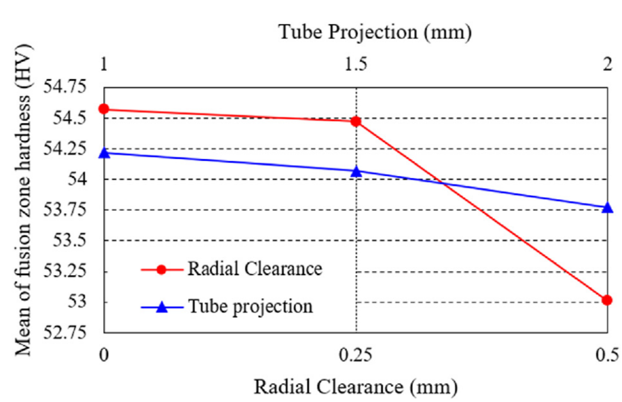

Fig. 14. Main effect plot of hardness at fusion zone.

Table 7
SN Ratios of response variables.

SI No.	Parameters		SN Ratio of Response Variables			
	Radial clearance	Projection	Load	Extension	Hardness: SZ	Hardness: FZ
1	0	1	78.27932	20.01562	−34.2412	−35.1408
2	0	1.5	74.28143	12.9633	−34.6992	−34.5979
3	0	2	80.0635[a]	22.85404[a]	−34.0244	−34.4647
4	0.25	1	75.63066	16.00609	−34.7677	−34.6506
5	0.25	1.5	79.68917	20.86803	−35.0302	−34.7462
6	0.25	2	75.82104	15.24907	−33.4819[a]	−34.7735
7	0.5	1	76.396	14.19727	−33.9927	−34.2333[a]
8	0.5	1.5	77.85266	17.3576	−34.7687	−34.6339
9	0.5	2	75.78866	15.66664	−33.8968	−34.5903
Optimum Conditions			**RC_1PL_3**	**RC_1PL_3**	**RC_2PL_3**	**RC_3PL_1**

[a] Denotes the optimum condition of radial clearance and projection length for individual characteristic responses.

results indicate minimal marginal difference at individual levels of tube projection and radial clearances. The mean hardness was reduced from 54.22 HV at 1 mm tube projection to 53.77 HV at 2 mm tube projection with a difference of 0.45 HV. On the other hand, the mean hardness at fusion zone at three levels of radial clearances at 0 mm and 0.25 mm was 54.57 HV and 54.47 HV, respectively. This indicates a constant and steady hardness value. Even though the hardness dropped to 53.01 HV at 0.5 mm radial clearance, the difference in the mean hardness from 1.5 mm to 2 mm radial clearance was 1.46 HV.

In comparison of FSWed and TIG welded tube to tube sheets, the highest hardness was found in the weld zone of TIG welded joint accounting up to an average of 67.17 HV. The improved hardness at the weld zone is caused by the presence of alloying element in the filler wire and faster cooling rate. The heat affected zone hardness at the tube and tube sheet are 61.17 HV and 64.02 HV respectively. The hardness at the weld zone and HAZ of TIG joint are found to be greater than the stirring and fusion zone of the FSWed joints. Therefore, friction stir welding is advantageous to reduce the brittleness and residual stress in the welded joints.

4.3. Single objective optimization

Single objective optimization was performed using the signal to noise ratio (S/N ratio) corresponding to the responses from the Taguchi analysis. The higher the load bearing capacity and extension, and lower the hardness at both of stirring zone and fusion zone are the preferred conditions. Table 7 shows the SN ratio of the responses. The optimal projection and radial clearance for exhibiting a maximum tube pull-out load of 100,073.37 N are 2 mm and 0 mm, respectively. The maximum extension was 13.89 mm where the corresponding projection was 2 mm and radial clearance was 0 mm. The least hardness at the stirring zone was 47.21 HV at 2 mm projection and 0.25 mm radial clearance. In fusion zone, the least hardness was 51.48 HV at 1 mm projection and 0.5 mm radial clearance. Therefore, based on single responses, the optimal combination of projection and radial clearances for load, extension, stirring zone hardness and fusion zone hardness are RC_1PL_3, RC_1PL_3, RC_2PL_3, RC_3PL_1.

Table 8
Eigenvectors corresponding to principal components.

Variable	PC1	PC2	PC3	PC4
GRC: Load	0.689	0.063	0.143	−0.708
GRC: Extension	0.679	−0.100	0.215	0.695
GRC: Stirring Zone Hardness	0.203	0.673	−0.702	0.116
GRC: Fusion Zone Hardness	0.153	−0.730	−0.664	−0.050

4.4. Multi-optimization using PCA-GRA

An integrated PCA-GRA for multi-response optimization uses unequal weights from principal component analysis to use in GRA for estimating grey relational grade. Four principal components with eigenvalues and eigenvectors are evaluated as shown in Table 8. The relative weights for each of the responses are obtained by squaring the eigenvectors of the first principal component [35]. The relative weights obtained by squaring the eigenvectors of the first PC were 0.474, 0.461, 0.0412, 0.0234. Table 9 illustrates the rank of set of parameters for the needed output. The optimal conditions in the case of GRA with equal weights of 0.5 were 1.5 mm projection and 0.25 mm radial clearance that exhibited 9648.472 N load (S/N ratio: 79.69), 11.05 mm extension (S/N ratio: 20.87), 56.43 HV hardness at stirring zone (S/N ratio: −35.03), 54.61 HV hardness at

Table 9
Ranks of GRA and PCA-GRA.

SI No.	Normalized			
	Load	Extension	Hardness: SZ	Hardness: FZ
1	0.691429	0.713022	0.490408	1
2	0	0	0.786213	0.401692
3	1	1	0.350413	0.254987
4	0.233348	0.307641	0.830447	0.45975
5	0.935261	0.799205	1	0.565186
6	0.266273	0.231102	0	0.595224
7	0.365713	0.12476	0.329913	0
8	0.617639	0.444284	0.83113	0.441423
9	0.260673	0.27332	0.267956	0.393369
SI No.	**Grey Coefficient**			
	Load	Extension	Hardness: SZ	Hardness: FZ
1	0.618375	0.635342	0.49525	1
2	0.333333	0.333333	0.700489	0.455246
3	1	1	0.434939	0.401602
4	0.394741	0.419337	0.746766	0.480654
5	0.885364	0.713475	1	0.534866
6	0.405276	0.394043	0.333333	0.552623
7	0.440805	0.363573	0.427318	0.333333
8	0.566662	0.473612	0.747529	0.472332
9	0.403445	0.407604	0.40583	0.451822
SI No.	**GRG**	**Rank**	**W-GRG**	**Rank W-GRG**
1	0.687242	3	0.15756	3
2	0.4556	6	0.087853	8
3	0.709135	2	0.240754	1
4	0.510375	5	0.105678	5
5	0.783426	1	0.200728	2
6	0.421319	7	0.100176	6
7	0.391258	9	0.100566	9
8	0.565034	4	0.132295	4
9	0.417175	8	0.101678	7

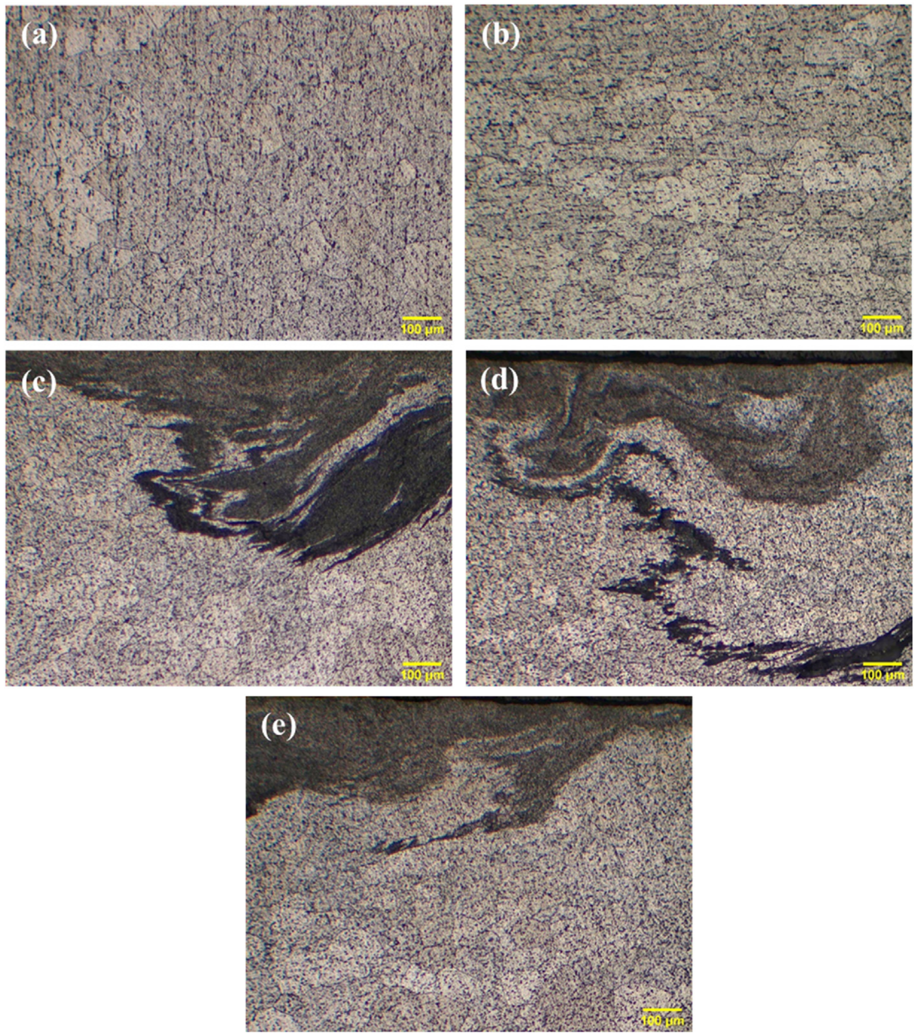

Fig. 15. Microstructure image of base materials at 100 times magnification: Base materials: (a) Tube, (b) Tube sheet, Stir Zone: (c) Tube, (d) Tube sheet, and (e) Fusion Zone.

fusion zone (S/N ratio: −34.74623876). The optimum projection and radial clearance were changed by assigning the relative weights from PCA. The optimum condition was 2 mm projection and 0 mm radial clearance for exhibiting 10,073.373 N load (S/N ratio: 80.06), 13.89 mm extension (S/N ratio: 22.85), 50.26 HV hardness at stirring zone (S/N ratio: −34.02), 52.87 HV hardness at fusion zone (S/N ratio: −34.46).

4.5. Microstructure analysis

Fig. 15(a) and (b) illustrate the microstructures of tube and tube sheet, respecively. The tube and tube sheet material exhibited coarse grains. In the conventional friction stir welding process where the tool pin and tool shoulder are used for stirring (similar geometry: pipe to pipe or plate to plate), the microstructures are known to significantly affect the nugget zone and thermo-mechanically heat affected zones [36]. However, in this research, the tool shoulder was mainly used for inducing frictional heat at the interface for effectively joining the tube to tube sheet (complex geometries). Whereas the FSW tool guide instead of a FSW tool pin was used for centering the tool to the welding specimens. A significant amount of friction at the interface between tool shoulder and tube-to-tube sheet specimen has caused an adequate material flow and grain structure evolution on the welded surface of tube and tube sheet forming a zone named “stir zone”. Under the action of the plunging and tool rotation, the softened plasticized material flowed and filled the clearance gap between the tube and tube sheet. This resulted in a friction stir welded TTSJ. The flow pattern as a result of the material flow is visible in the stir zone as shown in Fig. 15c and d. In addition, the stir zone comprised of finest grains on the sectioned weld cross-section. This peculiar nature of grains at the stir zone is in close agreement with the findings of Rupajati et al. that is finer grains are formed at the stir zone compared to thermo-mechanical heat affected zone and heat affected zone [37]. Fine grains are exhibited by the dynamic recrystallization initiated by the influence of intensive plastic deformation and temperature [38]. The clearance was filled with the softened material and the tube-to-tube sheet region of coalescence is named as “fusion zone”. The fusion zone as shown in Fig. 15e comprised of fine grains in regions close to tool-specimen interaction. While, coarse grains were observed in regions away from the tool-specimen interaction.

5. Conclusions

The main findings of this research and future scope are presented hereafter. Friction stir welding process is capable of achieving load bearing capacity of 10,073.37 N with a minimal difference of 8.47 N compared to tungsten inert gas welding process. Absence of radial clearance and higher tube projection are recommended for friction stir welded joints with high load bearing capacity and maximum extension. The optimal parameters for peak load, maximum extension, stirring zone hardness, fusion zone hardness by single objective Taguchi optimization are RC_1PL_3, RC_1PL_3, RC_2PL_3 and RC_3PL_1. The optimal geometrical conditions for producing quality friction stir welded joints using integrated Taguchi-PCA-GRA with unequal relative weights are 2 mm tube projection and 0 mm radial clearance. Fine grains are formed at the stirring zone due to tool-specimen interaction in the friction stir welding process. TIG welding imparted high hardness at the weld zone exhibiting 67.17 HV compared to FSW having maximum of 57.15 HV in the fusion zone. The further research gap is to investigate the friction stir welding of carbon steels using polycrystalline boron nitride tipped tool and the assessment of light expanded-seal welded TTSJ in the future. In addition, the penetrant test and minimum leak path are recommended to perform for the fabricated TTSJ according to ASME Section IX QW-288. The TEMA, ASME, NBIC, etc are preferred for the qualification of TTSJs.

CRediT authorship contribution statement

Dinu Thomas Thekkuden: Writing – original draft, Visualization, Validation, Resources, Methodology, Investigation, Formal analysis, Data curation. **Muhammad M. Sherif:** Writing – review & editing. **Mohammad Alkhedher:** Writing – review & editing. **Syed Haris Iftikhar:** Visualization, Resources, Methodology. **Abdel-Hamid Ismail Mourad:** Writing – review & editing, Validation, Supervision, Funding acquisition, Conceptualization.

Conflicts of interest

The authors declare that there is no conflicts of interest.

Acknowledgement and Funding

The project was funded and supported by United Arab Emirates University [Grant # 31R105].

References

[1] M.F. Saffiudeen, F.T. Mohammed, A. Syed, Comparative study of tube to tubesheet welding qualification on heat exchanger, J. Eng. Appl. Sci. 69 (2022) 1–14.
[2] D.T. Thekkuden, A.-H.I. Mourad, A.-H. Bouzid, Failures and leak inspection techniques of tube-to-tubesheet joints: a review, Eng. Fail. Anal. 130 (2021) 105798, https://doi.org/10.1016/j.engfailanal.2021.105798.
[3] S.E. Ibrahim, Impact of fatigue on tube-to-tubesheet welded joints in heat exchanger, J. Fail. Anal. Prev. 22 (2022) 1631–1636, https://doi.org/10.1007/s11668-022-01457-y.
[4] J. García González, J.J. Hernández-Ortega, A.-E. Jiménez-Ballesta, R.Z. Pedreño, Analysis of tube-to-tubesheet welding in carbon steel heat exchangers of a double plate header box, Materials 15 (2022) 261, https://doi.org/10.3390/ma15010261.
[5] A.-H.I. Mourad, A. Khourshid, T. Sharef, Gas tungsten arc and laser beam welding processes effects on duplex stainless steel 2205 properties, Mater Sci Eng A 549 (2012) 105–113, https://doi.org/10.1016/j.msea.2012.04.012.
[6] C.N. Patel, S. Chaudhary, Parametric optimization of weld strength of metal inert gas welding and tungsten inert gas welding by using analysis of variance and grey relational analysis, Int J Res Mod Eng Emerg Technol 1 (2013) 48–56.
[7] D.T. Thekkuden, A.-H.I. Mourad, A.-H. Bouzid, M.M. Sherif, Investigation of expansion percentages and groove inclusions on the performance of welded, expanded, welded-expanded tube-to-tubesheet joints, J. Mater. Res. Technol. 22 (2023) 2078–2092, https://doi.org/10.1016/j.jmrt.2022.12.045.
[8] G.H. Farrahi, K. Minaii, M. Chamani, A.H. Mahmoudi, Effect of residual stress on failure of tube-to-tubesheet weld in heat exchangers, Int. J. Eng. 32 (2019) 112–120.
[9] R. Sui, Y. Zhao, B. Ge, W. Wang, Failure analysis of leakage at tube-to-tubesheet joints of a waste heat boiler, Eng. Fail. Anal. 129 (2021) 105639, https://doi.org/10.1016/j.engfailanal.2021.105639.
[10] D.T. Thekkuden, A.-H.I. Mourad, T. Ramachandran, A.-H. Bouzid, R. Kumar, A. Alzamly, Combined effect of tungsten inert gas welding and roller expansion processes on mechanical and metallurgical characteristics of heat exchanger tube-to-tubesheet joints, J. Mater. Res. Technol. 21 (2022) 4724–4744, https://doi.org/10.1016/j.jmrt.2022.11.043.
[11] H.S. Patil, S.N. Soman, Experimental study on the effect of welding speed and tool pin profiles on AA6082-O aluminium friction stir welded butt joints, Int. J. Eng. Sci. Technol. 2 (2010) 268–275, https://doi.org/10.4314/ijest.v2i5.60163.
[12] G. Karrar, A.N. Shuaib, F.A. Al-Badour, N. Merah, A.K. Mahgoub, Friction Stir Butt Welding of Commercially Pure Copper Plates, American Society of Mechanical Engineers Digital Collection, 2015, https://doi.org/10.1115/IMECE2014-38378.
[13] H. Ma, Y. Wang, Z. Tian, L. Xiong, Y. Zhang, Gap-tolerance control for friction stir butt welding of 2A14 aluminium alloy, Measurement 148 (2019) 106915, https://doi.org/10.1016/j.measurement.2019.106915.
[14] Y. Yue, G. Wang, K. Yang, B. Wu, D. Yan, Friction stir butt welding thin aluminum alloy sheets, Int. J. Adv. Manuf. Technol. 96 (2018) 3139–3147, https://doi.org/10.1007/s00170-018-1798-z.
[15] A.-H.I. Mourad, M. Allam, A. El Domiaty, Study on the Mechanical Behavior of Aluminum Alloy 5083 Friction Stir Welded Joint, American Society of Mechanical Engineers Digital Collection, 2014, https://doi.org/10.1115/PVP2014-28556.
[16] I. Sabry, A.-H.I. Mourad, D.T. Thekkuden, Vibration-Assisted Friction Stir Welding of AA 2024-T3 Plates, American Society of Mechanical Engineers Digital Collection, 2021, https://doi.org/10.1115/PVP2021-62249.
[17] I. Sabry, A.-H.I. Mourad, D.T. Thekkuden, Study on Underwater Friction Stir Welded AA 2024-T3 Pipes Using Machine Learning Algorithms, American Society of Mechanical Engineers Digital Collection, 2022, https://doi.org/10.1115/IMECE2021-71378.
[18] I. Sabry, A.-H.I. Mourad, D.T. Thekkuden, Comparison of mechanical characteristics of conventional and underwater friction stir welding of AA 6063 pipe joints, Int Rev Mech Eng IREME 14 (2020) 64–70, https://doi.org/10.15866/ireme.v14i1.17483.
[19] B. Chen, K. Chen, W. Hao, Z. Liang, J. Yao, L. Zhang, et al., Friction stir welding of small-dimension Al3003 and pure Cu pipes, J. Mater. Process. Technol. 223 (2015) 48–57, https://doi.org/10.1016/j.jmatprotec.2015.03.044.
[20] A.M. El-Kassas, I. Sabry, Using Multi Criteria Decision Making in Optimizing the Friction Stir Welding Process of Pipes:A Tool Pin Diameter Perspective, vol. 14, 2019.
[21] A. Ismail, M. Awang, S.H. Samsudin, The influence of process parameters on the temperature profile of friction stir welded aluminium alloy 6063-T6 pipe butt joint, in: A. Öchsner, H. Altenbach (Eds.), Mech. Mater. Eng. Mod. Struct. Compon. Des, Springer International Publishing, Cham, 2015, pp. 243–249, https://doi.org/10.1007/978-3-319-19443-1_19.
[22] I. Sabry, D.T. Thekkuden, A.-H.I. Mourad, Topsis – GRA approach to optimize friction stir welded aluminum 6061 pipes parameters, 2022 Adv. Sci. Eng. Technol. Int. Conf. ASET (2022) 1–6, https://doi.org/10.1109/ASET53988.2022.9734821.
[23] I. Sabry, D.T. Thekkuden, A.-H.I. Mourad, K. Abdullah, Variants of friction stir welding for joining AA 6063 pipes, . S2022 Advci. Eng. Technol. Int. Conf. ASET (2022) 1–4, https://doi.org/10.1109/ASET53988.2022.9735118.
[24] Castro RAS, Richter-Trummer V, Tavares SMO, Vilaça P. Friction Stir Welding on T-Joints: Residual Stress Evaluation (n.d).
[25] A.C.F. Silva, D.F.O. Braga, MAV de Figueiredo, P.M.G.P. Moreira, Friction stir welded T-joints optimization, Mater. Des. 55 (2014) 120–127, https://doi.org/10.1016/j.matdes.2013.09.016.
[26] A. Daniel Das, K. Thirunavukkarasu, Parametric optimization of FWTPET for optimum tensile strength by genetic algorithm approach, Mater. Today Proc. 37 (2021) 1571–1577, https://doi.org/10.1016/j.matpr.2020.07.159.
[27] S. Senthil Kumaran, S. Muthukumaran, C. Chandrasekhar Reddy, Suitability of friction welding of tube to tube plate using an external tool process for different tube diameters—a study, Exp. Tech. 37 (2013) 8–14, https://doi.org/10.1111/j.1747-1567.2011.00765.x.
[28] S.S. Kumaran, S. Muthukumaran, Effect of projection on joint properties of friction welding of tube-to-tube plate using an external tool, Int. J. Adv. Manuf. Technol. 75 (2014) 1723–1733, https://doi.org/10.1007/s00170-014-6269-6.
[29] D.T. Thekkuden, A.-H.I. Mourad, S.H. Iftikhar, R. Krishnapriya, Friction stir weld processing for achieving maximum tube-to-tubesheet leak path, Mater. Manuf. Process. 38 (2023) 1455–1461, https://doi.org/10.1080/10426914.2023.2176874.
[30] E. Radhakrishnan, L.A. Kumaraswamidhas, D. Muruganandam, S.S. Kumaran, Dissimilar metal study on C44300 tube to AA7075 -T651 tube plate with and without thread by FWTPET process, J. Mech. Sci. Technol. 31 (2017) 2523–2533, https://doi.org/10.1007/s12206-017-0450-4.
[31] S. Kannan, S. Senthil Kumaran, L.A. Kumaraswamidhas, An investigation on mechanical property of commercial copper tube to aluminium 2025 tube plate by FWTPET process, J. Alloys Compd. 672 (2016) 674–688, https://doi.org/10.1016/j.jallcom.2016.02.205.
[32] L. Long, X. Zhang, S. Gu, X. Li, X. Cheng, G. Chen, Experimental and simulation investigation on fatigue performance of H13 steel tools in friction stir welding of aluminum alloys, Materials 17 (2024) 1535, https://doi.org/10.3390/ma17071535.
[33] C.K. Sivakumar, Y. Robinson, P. Prema, S. Joe Patrick Gnanaraj, M. Appadurai, Mechanical characteristics of aluminium alloy joints produced by friction stir welding, Mater. Today Proc. 62 (2022) 5620–5624, https://doi.org/10.1016/j.matpr.2022.04.831.

[34] Aluminum mig wires/tig rods (gmaw/gtaw) n.d. https://esab.com/mv/ind_en/products-solutions/filler-metals-pdf/?filename=mdm-productfamily-29342&siteid=ind_en&countryname=IND&countrylocale=en-in.
[35] M.I. Qazi, R. Akhtar, M. Abas, Q.S. Khalid, A.R. Babar, C.I. Pruncu, An integrated approach of GRA coupled with principal component analysis for multi-optimization of shielded metal arc welding (SMAW) process, Materials 13 (2020) 3457, https://doi.org/10.3390/ma13163457.
[36] A. Banik, A. Saha, J. Deb Barma, U. Acharya, S.C. Saha, Determination of best tool geometry for friction stir welding of AA 6061-T6 using hybrid PCA-TOPSIS optimization method, Measurement 173 (2021) 108573, https://doi.org/10.1016/j.measurement.2020.108573.
[37] P. Rupajati, K.G. Clarissa, A.S. Baskoro, G. Kiswanto, Characteristics of Mechanical Properties and Microstructure of Micro Friction Stir Spot Welding of AA1100 and Brass, International Journal of Technology 12 (2021) 1302–1311, https://doi.org/10.14716/ijtech.v12i6.5214.
[38] P. Yu, C. Wu, L. Shi, Analysis and characterization of dynamic recrystallization and grain structure evolution in friction stir welding of aluminum plates, Acta Mater. 207 (2021) 116692, https://doi.org/10.1016/j.actamat.2021.116692.